Droplet Deformation and Pumping in AC Electro-Osmotic Micropumps

Bernhard WEISS [1,*], Wolfgang HILBER [2], Philipp GITTLER [1], Bernhard JAKOBY [2]

* Corresponding author: Tel.: ++43 732 2468 9774; Fax: ++43 732 2468 9783; Email:
bernhard.weiss@jku.at
1 Institute of Fluid Mechanics and Heat Transfer, Johannes-Kepler University Linz, AUT
2 Institute for Microelectronics and Microsensors, Johannes-Kepler University Linz, AUT

Abstract This contribution deals with the pumping and deformation of oil in water droplets in alternating-current electro-osmotic micropumps. These micropumps are used to transport lowly conductive fluids through micro channels by means of a harmonically driven electrode array on the channel bottom. The periodic formation of an electric double layer above the electrodes results in an electro-osmotic flow, which carries along adjacent fluid layers. In experiments we observed that droplets immersed in the carrier fluid are transported by the channel flow and periodically deformed when passing the electrodes. Due to the different polarizability and conductivity of the droplet and the carrier fluid, dielectrophoretic forces act on the fluid-droplet interface. These forces that are described by the Maxwell stress tensor increase with the electric field strength and attract the droplet towards the electrode. This contribution analyses the mechanisms of droplet pumping and deformation numerically by means of solving for the electric and the flow field to the two phases in the channel and by evaluating the dielectrophoretic forces on the droplet. A conservative level-set method is used to track the droplet surface accurately.

Keywords: Droplet Deformation, AC Electro-Osmotic Micropump, Dielectrophoresis, Level-Set Method

1. Introduction

In micro-fluidic devices as e.g. lab-on-a-chip devices a common task is the transport of liquids and immersed particles, droplets or cells. For the flow-generation through micro channels traditionally pumps with movable parts where used. With the aim of transporting fluids without the use of classical pumps, electro-kinetic effects have found be of great potential. Among these, the electro-osmotic (EO) flow describes the movement of charged fluid layers along charged walls due to an applied transversal electric field. It results in a plug-like flow but requires high electric fields of several kV/m. Recent publications recommend the use of periodic interdigitated electrode arrays with a length scale of some micrometers to reach these field strengths with applied voltages of a few volts (Ajdari, 2000). Alternating-current electro-osmotic (ACEO) micropumps consist of a rectangular channel with an interdigitated electrode array on the bottom. A device, which is built in SU8 technology by means of photolithography and a lift off process for the titanium electrodes (Hilber et al. 2008), is shown in Fig. 1. The pumping mechanism is based on the periodic formation of an electric double layer (EDL), which inhomogeneously screens the electrodes. EO flow results from the transport of charged fluid layers by the remaining tangential electric field.
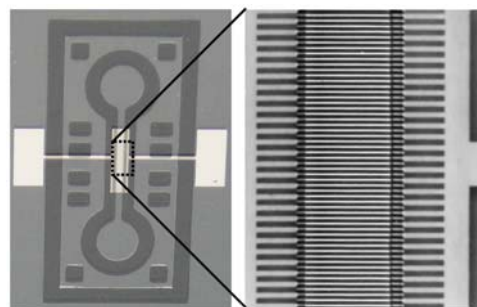

Fig. 1. Picture of the completed chip with a detailed view on the ACEO pump structure in the fluid channel. Distance between the fluid reservoirs is 10 mm.

Droplets and particles immersed in the EO channel flow are dragged along by viscous forces and influenced by gravitational and electric forces due to the remaining inhomogeneous electric field in the bulk of the

channel (Weiss et al. 2008). Depending on the polarizability and the conductivity of both, the carrier fluid and the droplet, it is pushed away from areas of high electric fields or attracted to them, which is known as dielectrophoresis. The interplay of dielectrophoretic (DEP), viscous shear, surface tension and gravitational forces affect the pumping dynamics of immersed droplets (Wang et al. 1997).

Experimental observations with the pumping of the compartments of a lubrication emulsion in water with the above device have shown interesting periodic droplet deformation, which is depicted in Fig. 2.
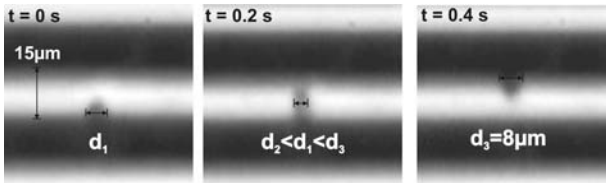

Fig. 2. Extracted pictures from a video taken with an ocular CCD of an oil-like drop in water being transported in an ACEO micropump. The fingers of the interdigitated electrode array on the channel bottom appear as white rectangles. When passing a finger the droplet is stretched significantly, such that its thickness decreases from 8µm to 4.5µm. The driving frequency was 1 kHz and the applied peak voltage was 4 V.

When passing over an electrode, the droplet is significantly stretched. The aim of this contribution is the investigation of the droplet dynamics in order to explain droplet deformation an especially the influence of the harmonic electric field on its shape. Therefore, the droplet motion is computed by means of the finite element method. Section 2 and 3 describe the modeling of the EO flow and analyze the resulting channel flow. Section 4 and 5 finally deal with the modeling and analysis of the droplet dynamics.

2. Modeling of the EO flow

2.1 Electric problem

The accumulation of ions of an electrolytic fluid beside a charged wall results in an EDL beside the wall. It consists of a Stern layer - a single layer of ions, which adhere to the electrode - and a movable diffuse layer, where diffusion forces due to thermal motion

balance electric attraction. A common approach for the computation of the EDL development and the resulting EO flow is the thin double layer theory. For a symmetric fluid of density ρ_f, viscosity μ_f, ion concentration c_0, dielectric permittivity ε_f and conductivity σ_f the characteristic length for the extension of the diffuse layer is defined by the Debye length (Ajdari, 2000)

$$\lambda_d = \sqrt{\frac{\varepsilon_f k_b T}{(z e_0)^2 c_0}} \,, \qquad (1)$$

where k_b, T, z and e_0 are the Boltzman constant, the temperature of the fluid, the ion valence and the elementary charge, respectively. For lowly conductive fluids λ_f is in the order of a few nanometers. Consequently, in microfluidic environments the EDL is thin compared to the channel extension. Furthermore the thin EDL theory assumes that (1) the equilibrium bulk ion concentration is not influenced by the EDL formation, that (2) the accumulated ions can be quantified by a net surface charge q at the fluid–electrode interface. This permits that (3) the EDL formation can be described by charging a capacity of an equivalent electric circuit, where respective surface capacities C_S and C_D for the Stern and the diffuse layer are charged through the bulk fluid, which corresponds to a resistance characterized by its conductivity σ_f (Ajdari 2000 and Green et al. 2002). For low EDL charging these capacities are constant and the capacity of the DL is

$$C_{DL} = \left[C_S + C_S \right]^{-1} = \frac{\varepsilon_f}{\lambda_d (1+\delta)}, \qquad (2)$$

where δ is the relation of the Stern layer thickness to the diffuse layer thickness.

The EDL formation and the field description can be summarized as follows. The electric field in the source free symmetric electrolyte is described by the Laplace equation

$$\Delta \phi = 0 \,, \qquad (3)$$

where ϕ is the electric potential. At the electrode fluid interface the following boundary condition describes the accumulation of the

charge q in the EDL:

$$\frac{\partial q}{\partial t} = -\vec{n} \cdot \vec{E}, \qquad (4)$$

where $\vec{n}$ and $\vec{E}$ are the normal vector of the boundary pointing into the channel and the electric field is $\vec{E} = -\nabla\phi$. A voltage $V_{app} = V_0 \sin\left(2\pi f_{dr} t + \varphi_i\right)$ of amplitude V_0 and driving frequency f_{dr} is applied to the electrodes. Here, φ_i is $\pi/2$ for every second electrode, indicating that neighboring electrodes are antipodally driven. Finally, the potential at the outside of the EDL serves as boundary condition for the electric field:

$$\varphi_0 = V_{app} + \frac{q}{C_{DL}}. \qquad (5)$$

The electric problem is linear in case that the DL capacity is constant and independent from q , which is the case if $q < C_D \cdot 25mV$.

2.2 Flow problem

The charge accumulation in the mobile diffuse layer is quantified by the zeta-voltage $\zeta = q/C_D$. In the presence of an electric field component tangential to the electrode $\vec{E}_t$ the charged diffuse layer is dragged along by Coulomb forces. The velocity, which is reached by the outer layer of the diffuse layer, is called Helmholz-Smoluchowski electro-osmotic slip velocity:

$$\vec{u}_s = \varepsilon_f \frac{\zeta}{\mu_f} \vec{E}_t. \qquad (6)$$

This slip velocity serves as a boundary condition for the flow problem (Green el al. 2002). The fluid flow is described by the Navier-Stokes equations being the conservation of mass and momentum. Considering that in the micro-fluidic flow regime viscous shear forces dominate over inertial forces, for an incompressible fluid these equations reduce to

$$\nabla \cdot \vec{u} = 0,$$
$$0 = -\nabla p + \nabla \cdot \left[\mu_f \nabla\vec{u} + \mu_f \left(\nabla\vec{u}\right)^T \right], \qquad (7)$$

where p and $\vec{u}$ are the pressure and the vector of the fluid velocity. We apply the slip velocity as a boundary condition for the electrodes, the no-slip condition to the channel walls and periodic boundaries, as we only want to compute the flow over one pair of electrodes in the array.

In electro-osmotic flows, the time-scale of the driving voltage is far below the time-scale of the fluid flow. Consequently, time-averaged values of the slip velocity can be used as boundary for the static fluid computation. We regard a harmonic driving voltage and consequently, the potential ϕ is also harmonic $\phi(t) = \text{Re}\left\{\bar{\phi} e^{j2\pi f_{dr} t}\right\} = \left(\bar{\phi} + \bar{\phi}^*\right)/2$, where the over-line indicates a complex value and $\bar{\phi}^*$ is the conjugate complex value of $\bar{\phi}$. The time-averaged slip-velocity is finally $\vec{u}_{s,av} = \varepsilon_f \text{Re}\left\{\bar{\zeta} \bar{\vec{E}}_t^*\right\}/2\mu_f$.

2.3 Numerical solution

In the computation of the electro-osmotic channel flow the electric and the flow problem are exclusively coupled by the slip-velocity $\vec{u}_{s,av}$, which results from the solution of the electric problem. Consequently, the electric problem is solved primarily, resulting in the slip-velocity for the subsequent computation of the flow problem.

3. Analysis of the channel flow

Let us now look at the resulting electric and flow field above a pair of electrodes, when the electrode array is driven with a voltage V_0 of 2 V and a frequency f_{dr} of 1 kHz. The used liquid is DI water with a conductivity of 20 µS/m.

3.1 Electric field

Figure 3 shows us, that the EDL is mainly charged above the edges of the electrodes where the electric field is strongest. Due to the inhomogeneity of the EDL charging an electric field component $\vec{E}_t$ arises, which is parallel to the electrodes. In spite of the EDL charging the electric field gradient is highest above the electrode edges.
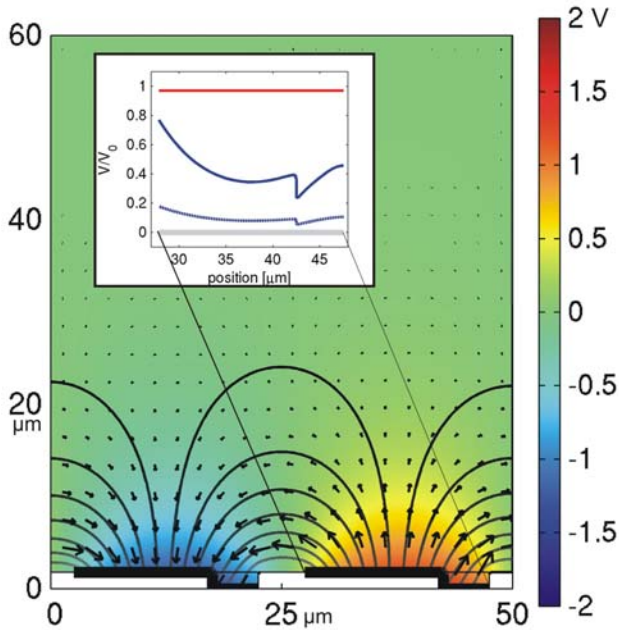
Fig. 3. Big plot: Electric potential, the lines and arrows of the electric field and the double layer charging at the moment of maximum spatially averaged slip above a pair of electrodes. Small plot: Voltage drops across the Stern layer (dashed blue), voltage drop across the diffuse layer (blue minus blue dashed line) and the potential at the electrode (red).

3.2 Flow field

The remaining electric field is inhomogeneous and moves the EDL above the electrodes through Coulomb forces which results in an electro-osmotic slip. This flow velocity scales with the charging of the diffuse layer – characterized by ζ - and the trans-versal electric field. Consequently, the EO-slip is highest at the electrode edges and points towards the electrode centres – see Fig. 4. In the case of a planar symmetric electrode array, two swirls above each electrode would result, that would cancel out each other. Lowering the right part of the electrode effects that the swirl above this lowered part supports the flow caused by the left electrode part in stead of cancelling it (Urbanski et al. 2007). The resulting flow above this electrode configu-ration is characterized by a periodic wavelike shape with vertices that concentrate on the electrode edges.

4. Modeling of the droplet motion

Computing the motion of a droplet in the ACEO channel flow corresponds to a two-phase computation. One possible solution would be the modeling of the droplet as a separate computational domain with a proper system of equations. At each time step the fluid-droplet interface would have to be updated, by evaluating the stresses, evolving the interface and by remeshing the problem. In this work we follow an Eulerian approach using the level-set method of Olsson et al. (2007).
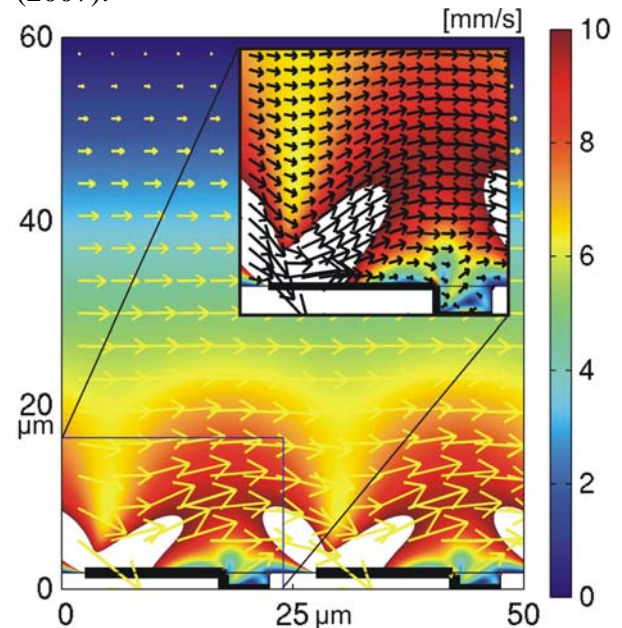

Fig. 4. Contours of the amplitude and arrows of the resulting channel flow. The small plot shows the detailed flow above one electrode, where we can see a swirl above the lowered electrode part which enforces the net flow through the channel.

4.1 Level-set method

In the whole computational domain the scalar field ψ - called level-set function (LSF) - describes whether this point is part of the carrier fluid ($\psi = 0$) or part of the droplet ($\psi = 1$). The $\psi = 0.5$ level defines the fluid-droplet interface. In order to compute interfacial forces accurately, a smooth transition of the LSM from 0 to 1 has to be assured. The motion of the droplet corresponds to the advection of the LSM with the fluid velocity:

$$\frac{\partial \psi}{\partial t} + \nabla.\left(\vec{u}\psi\right) = 0 \,. \qquad (8)$$

The LSF is initialized with a sine-function regarding a smooth transition at the interface. In the course of the droplet deformation the

LSF gets distorted, which corrupts the computation of interfacial forces such as surface tension. In order to avoid this, the LSF has to be regularly reinitialized. As reinitialisation procedure, which conserves the droplet volume, the equation

$$\frac{\partial \psi}{\partial t} + \nabla \cdot \left(\psi(1-\psi)\vec{n} \right) = \alpha \nabla \cdot \left((\nabla \psi \cdot \vec{n})\vec{n} \right) \quad (9)$$

is solved to steady state. Here, α is a diffusion constant and affects the width of the transition thickness of the interface, and $\vec{n} = \nabla \psi_{\hat{t}=0} / \left| \nabla \psi_{\hat{t}=0} \right|$ is the unit normal vector on the interface at beginning of the reinitialisation procedure.

For the computation of electric and flow fields in the carrier fluid and the drop the upper Laplace the Navier-Stokes equations can be used regarding the properties

$$\mu = \mu_f + \psi(\mu_d - \mu_f) \quad (10)$$

and analogous equations for the permittivity, the density and the conductivity of the both phases. Here, the subscript d is used to describe the properties of the droplet.

4.2 Fluid forces

As the droplet and the carrier fluid have different interfacial tensions, a surface tension force has to be regarded in the momentum balance

$$\vec{F}_{st} = \gamma \kappa \delta(\psi)\vec{n}$$
$$= -\gamma \underbrace{\left(\nabla \cdot \frac{\nabla \psi}{|\nabla \psi|} \right)}_{\kappa} 6|\psi(1-\psi)| \nabla \psi, \quad (11)$$

where κ and γ are the curvature of the droplet surface and the surface tension coefficient.

4.3 Electric forces – Maxwell Stress Tensor

In the presence of an electric field, both the droplet and the carrier fluid are polarized. If the permittivity of the fluid and the droplet are different, an effective electric dipole moment results, that acts as a force on the drop surface. In the case of conductive fluids beside the displacement current also conduction current

influences this force as free charge carriers accumulate at the fluid droplet interface. The Maxwell stress-tensor (MST) couples these electric forces to the momentum balance of both phases (Wang et al. 1997):

$$\underline{T}_M = \varepsilon \vec{E} \otimes \vec{E} - \frac{1}{2} \varepsilon \left(\vec{E} \cdot \vec{E} \right) \underline{I}, \quad (12)$$

where $\underline{I}$ is the unit matrix and $\otimes$ is the dyadic product. Regarding that the time-scale of the electric problem vanishes compared to the fluid flow, we use the time-averaged MST in the momentum balance

$$\underline{T}_{M,av} = \frac{1}{4} \mathrm{Re} \{ \overline{\varepsilon} \} \left[\left(\vec{E} \otimes \vec{E}^* + \vec{E}^* \otimes \vec{E} \right) \right.$$
$$\left. - \left(\vec{E} \cdot \vec{E} \right) \underline{I} \right] \quad (13)$$

and compute the electric field with

$$\nabla \cdot \left(\overline{\varepsilon} \nabla \overline{\phi} \right) = 0. \quad (14)$$

In this equation, $\overline{\varepsilon} = \varepsilon - i \left(\sigma / 2\pi f_{dr} \right)$ describes the complex permittivity, which accounts for both polarization and for the ion accumulation at the fluid-drop interface due to conduction currents that scale with the conductivity σ.

Regarding the time-averaged MST and the surface tension force in the momentum equation yields in dimension-less form (Singh et al. 2007)

$$0 = -\nabla' p' + \frac{1}{\mathrm{Re}} \nabla' \cdot \left[\mu' \nabla' \vec{u}' + \mu' \left(\nabla' \vec{u}' \right)^T \right]$$
$$+ \frac{1}{\mathrm{Re\,Ca}} \kappa' \delta'(\psi)\vec{n} + \frac{1}{\mathrm{Re\,Ma}} \frac{r}{l} \nabla' \cdot \underline{T}'_{M,av} \quad (15)$$
$$+ \frac{1}{\mathrm{Fr}^2} (1 - \rho').$$

Here, $\mathrm{Re} = \rho_f u_0 r / \mu_f$ is the Reynolds number, which describes the ratio of inertial to viscous forces in the carrier fluid. The Froude number $\mathrm{Fr} = u_0 / \sqrt{gl_0}$ quantifies the influence of gravity and buoyancy forces. The capillary number $\mathrm{Ca} = u_0 \mu_f / \gamma$ describes the ratio of viscous to surface tension forces. Finally, the Mason number $\mathrm{Ma} = \mu_f u_0 / \varepsilon_f r \beta^2 E_0^2$ is the ratio of viscous to electric forces. The adapted Weber number

$We = Ma / Ca$ quantifies the droplet deformation due to dielectrophoretic forces. In these dimensionless numbers r, l_0, u_0 and E_0 are the radius of the undeformed spherical droplet, the characteristic width of an electrode, the spatially averaged slip velocity and the characteristic electric field strength V_0 / l_0, respectively.

4.4 Solution procedure

The transient problem comprises the electric field, the flow solution and the convection and regular reinitialisation of the LSF. Thereby, the only time-dependent term occurs in the convection equation. The problem is solved in three dimensions with the commercial finite element solver Comsol Multiphysics 3.5 using Matlab 7 as programming interface. As a transient coupled solution of the system was not possible a sequential solution was used. The convection equation was solved transiently, where the electric and the flow field where regularly updated.

5. Analysis of the droplet motion

This section analyses the electric and the flow field around an 12 μm droplet immersed in water, which is characterized by a density of $\rho_d = 880 \, kg \, m^{-3}$, a viscosity of $\mu_d = 80 \, mPa \, s$, an interfacial surface tension of $\gamma = 48 \, mN / m$ and a conductivity of $\sigma_d = 65 \, mS / m$. In this case the Weber number is We=0.013.

5.1 Numerical issues

The computations where performed on a two core work station with 2x2.6 GHz and 6 GB of RAM. Using a computational mesh with 7100 hexahedral elements and Lagrangian elements of second order for all values besides the pressure, the computation of the unique droplet motion over the electrode pair took about 13 hours. The complex dynamics at the fluid-droplet interface would require more computational accuracy, by using elements of higher order or adaptive mesh refinement at the interface. Respective adaptations have not been possible due to limited computational resources. Nevertheless, the following results reproduce the interface dynamics quite well.

5.2 Electric field

Figure 5 shows the electric potential and the electric field lines corresponding to the Fig. 3 without an immersed droplet. In comparison to the carrier fluid, the drop acts like a conductor as its conductivity is several orders higher than the conductivity of the carrier fluid. Consequently, free ionic charges dispersed in the droplet accumulate at the fluid-droplet interface due to an initial electric field until the potential in the droplet is constant and the local electric field in the droplet vanishes.
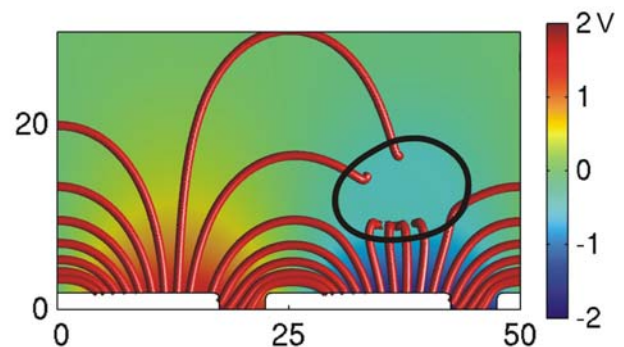

Fig. 5. Electric potential and electric field lines at the moment where the electrodes have a potential of $\pm V_0$ in the plane of symmetry of the droplet, i.e. indicated by the contour.

5.3 Flow field

Investigating the channel flow in the presence of an immersed droplet, shown in Fig. 6, yields the following:
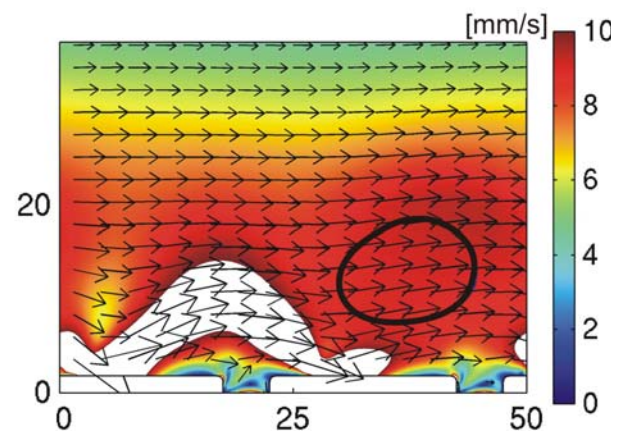

Fig. 6. Contours of the amplitude and vectors of the resulting EO channel flow in the case of an immersed droplet (corresponding to Fig. 4) in the plane of symmetry of the droplet, i.e. indicated by the contour.

(1), the velocity in the droplet is almost constant is its shape deforms only little in the periodic motion. (2), the velocity peak above right electrode is hindered by the slowly propagating droplet. And (3), the conductive droplet causes an increase of the electric field and consequently the averaged resulting slip velocity is 12 % higher than in the channel flow without the droplet (see Fig. 4).
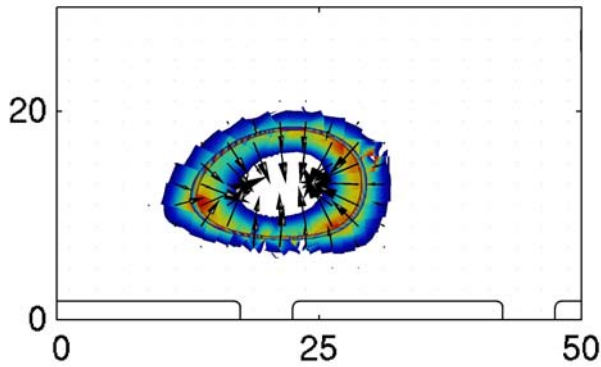
5.4 Interfacial forces

Fig. 7. Amplitude and vectors of the surface tension forces. They act on the smooth phase transition and push especially highly deformed interfaces characterized by a high curvature towards the centre of the droplet.

The droplet deformation is directly related to the present interfacial forces, namely viscous shear forces, surface tension and dielectrophoretic forces. Surface tension scales with the curvature of the surface and consequently pushes the droplet back towards a spherical shape, as it can be observed in Fig. 7.
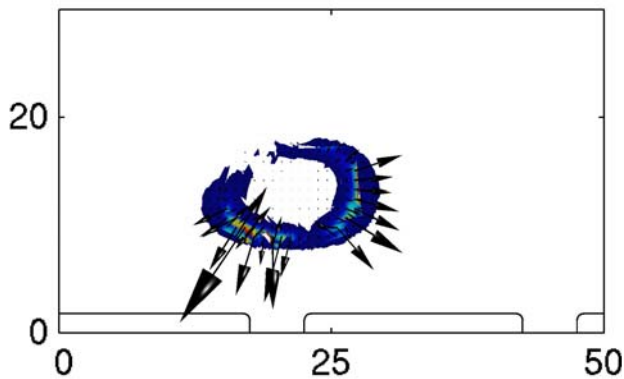

Fig. 8. Amplitude and vectors of the dielectro-phoretic forces on the phase transition.

Contrariwise, dielectrophoretic forces on the fluid-droplet interface in Fig. 8 point out of the droplet and deform it. Looking at the MST shows us that this interfacial force scales with

the square of the electric field strength. Consequently, dielectrophoretic forces are highest near the electrode edges and push the particle toward the areas of high electric fields, which is called positive dielectrophoresis. In the case of a high driving frequency or a vanishing conductivity of the droplet, negative dielectrophoretic forces would push the droplet away from the electrodes.
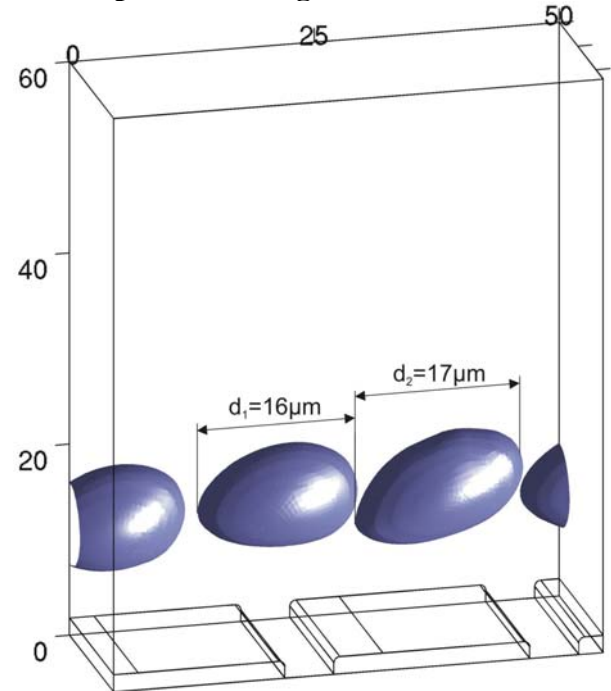
5.5 Droplet stretching

Fig. 9. Shape of the 12 µmm droplet in water at three different times.

Figure 9 shows the shape of the 12 µm droplet at three different moments. We notice a strong elongation of the droplet from 12 µm of the undeformed state to 17 µm. This lateral elongation is strongest, when the droplet moves above the upper step of the electrode. The elongation is smallest between two electrodes. Furthermore, it appears that the vertical motion of the droplet is small, which indicates that the vertical dielectrophoretic force is in the order or the buoyancy force. The elongation of the drop is caused both by viscous shear forces and lateral dielectrophoretic forces, which are oriented towards the electrode edges. These interrelations correspond to the observations shown in Fig. 2.

6. Conclusions

This work analyzes the mechanisms of pumping and deformation of oil-like droplet in water in ACEO micropumps by means of finite element computations. The modeling of the two-phase flow comprises the thin double layer approach for the EO flow, the level-set method to describe the fluid-droplet interface and the Maxwell stress tensor for coupling the interfacial electric forces to the fluid motion. Computations have shown that special attention has to be drawn to the mesh quality at this interface, which could not be resolved satisfactory in the current computations. Even so, important insight into the interface dynamics could be achieved.

The computations have shown that the electrical problem is dominated by the conductivity of the droplet. Due to the initial electric field ions accumulate at the droplet surface such that the electric field inside the droplet is cancelled out. The resulting increase of the electric field at the droplet-fluid interface causes strong dielectrophoretic forces that attract the droplet surface towards the edges of the driving electrodes. The interplay with the surface tension forces and viscous shear forces caused by the electro-osmotic channel flow, determines the periodic motion and deformation of the droplet when passing the electrodes. In the current configuration the droplet is stretched by viscous and lateral dielectrophoretic forces. The maximum elongation occurs when the droplet passes the higher part of an electrode, which is in agreement with experimental observations.

This work shows that the applied modeling is fully capable of describing the motion and interface dynamics of droplets. Further developing the modeling will finally make this method applicable to cell dynamics.

Nomenclature:

symbol	unit	description
C	$C\,m^{-2}$	surface cap. of the EDL
c_0	m^{-3}	equilibrium ion concentr.
E	$V\,m^{-1}$	electric field
f_{dr}	s^{-1}	frequency of V_{app}
p	$N\,m^{-2}$	pressure
q	$C\,m^{-2}$	surface charge density
$\vec{u}$	$m\,s^{-1}$	fluid velocity
$\vec{u}_s$	$m\,s^{-1}$	EO slip velocity
V_{app}	V	applied voltage
V_0	V	magnitude of V_{app}
δ	1	ratio of diff. and Stern layer
ε_f	$A\,s\,V^{-1}m^{-1}$	permittivity of carrier fluid
ϕ	V	potential
γ	$N\,m^{-1}$	surface tension
κ	m^{-1}	curvature
λ_d	m	Debye length
μ	$kg\,m^{-1}s^{-1}$	dynamic viscosity
ρ	$kg\,m^{-3}$	mass density
σ	$S\,m^{-1}$	conductivity
ψ	1	level set function
ζ	V	voltage drop over diff. layer
γ	$N\,m^{-1}$	surface tension

References:

Ajdari, A., 2000. Pumping liquids using asymmetric electrode arrays. Phys. Rev. E 61(1),R45–R48.

Green, N.G., Ramos, A., Gonzalez, A., Morgan. H., Castellanos, A., 2002. Fluid flow induced by nonuniform AC electric fields in electrolytes on microelectrodes. III. Observation of streamlines and numerical simulation. Phys. Rev. E 66(2):026305.

Hilber, W., Weiss, B., Mikolasek, M., Holly, R., Hingerl, K., Jakoby, B., 2008. Particle manipulation using 3D AC electro-osmotic micropumps, J. Micromech. Microeng. 18:6.

Olsson, E., Kreiss, G., Zahedi, S., 2007. A conservative level set method for two phase flow II. Jour. Comp. Phys. 225, 785-807.

Singh, P., Aubry, N., 2007. Transport and deformation of droplets in a microdevice using dielectrophoresis. Electrophor., 28, 644-657.

Urbanski, J.P., Levitan, J.A., Burch, D.N., Thorsen, T., Bazant, M.Z., 2007. The effect of step height on the performance of threedimensional AC electro-osmotic microfluidic pumps. J. Coll. Interf. Sci. 309(2):332–341.

Wang, X., Wang, X.B., Gascoyne, P.R.C., 1997. General expressions for dielectrophoretic force and electrorotational torque derived using the Maxwell stress tensor method. Jour. Electrost., 39, 277-295.

Weiss, B., Hilber, W., Holly, R., Gittler, P., Jakoby, B., Hingerl, K., 2008. Dielectrophoretic particle dynamics in alternating-current electro-osmotic micropumps. Appl. Phys. Lett. 92(18), 184101.